Underdense relativistically thermal plasma produced by magnetically assisted direct laser acceleration

K. Weichman [1,2,*] J. P. Palastro [1] A. P. L. Robinson,[3] R. Bingham,[3,4] and A. V. Arefiev [2,5]

[1]*Laboratory for Laser Energetics, University of Rochester, Rochester, New York 14623, USA*
[2]*Department of Mechanical and Aerospace Engineering, University of California at San Diego, La Jolla, California 92093, USA*
[3]*Central Laser Facility, STFC Rutherford-Appleton Laboratory, Didcot OX11 0QX, United Kingdom*
[4]*Department of Physics, SUPA, University of Strathclyde, Glasgow G4 0NG, United Kingdom*
[5]*Center for Energy Research, University of California at San Diego, La Jolla, California 92037, USA*

We introduce the first approach to volumetrically generate relativistically thermal plasma at gas-jet-accessible density. Using fully kinetic simulations and theory, we demonstrate that two stages of direct laser acceleration driven by two laser pulses in an applied magnetic field can heat a significant plasma volume to multi-MeV average energy. The highest-momentum feature is 2D-isotropic, persists after the interaction, and includes the majority of electrons, enabling experimental access to bulk-relativistic, high-energy-density plasma in an optically diagnosable regime for the first time.

*Corresponding author: kweic@lle.rochester.edu

The discovery of special relativity in 1905 transformed the fields of electromagnetism and charged particle kinetics that, some twenty years later, would coalesce into the field of plasma physics. Plasmas in which the majority of electrons are relativistic regardless of reference frame are found, for example, in astrophysics, where predictions have continually emphasized the importance of special relativity. However, the terrestrial study of relativistic effects has been constrained by the inaccessibility of large-volume, bulk-relativistic plasma that remains hot without concurrent laser drive. The laboratory generation of persistent, relativistically thermal plasma under optically diagnosable conditions is predicted to enable new regimes in plasma physics associated with substantial modification of the plasma response to electromagnetic radiation relative to the nonrelativistic or nonthermal cases, and is of significant interest in basic plasma physics [1], laboratory astrophysics [2,3], and laser-plasma physics [4–7]. In addition, laser interaction with already-relativistic plasma offers laboratory analogs for astrophysical phenomena including particle acceleration [8–10], maser emission [11], and proposed mechanisms for fast radio bursts [12].

The laboratory production of relativistically thermal plasma suitable for applications is complicated by the need to heat a large plasma volume while preventing charge separation return current from spoiling the bulk-relativistic electron distribution. Laser pulses with relativistic intensity ($I_0 \gtrsim 10^{18}$ W/cm^2 for $\lambda_0 = 1$ μm wavelength) are capable of imparting relativistic energy to electrons, however, in configurations involving opaque plasma ($n_e > n_c$, where $n_c \approx 10^{21}$ cm^{-3} is the critical density for $\lambda_0 = 1$ μm) [13–15] and near-critical density plasma [16], heating is limited to small spatial regions due to either the target structure or filamentation. These configurations are also subject to significant return current and are challenging to optically probe. In the underdense regime ($n_e < n_c$), laser-driven plasma (wakefield) electric fields can trap and accelerate electrons [17,18], but leave the majority of the population cold. Direct laser acceleration, on the other hand, volumetrically accelerates electrons to high energy [19,20], but imparts negligible lasting energy to electrons due to the reversibility of the acceleration process. This reversibility is disrupted, however, by the addition of a uniform static magnetic field, enabling dramatic plasma heating.

In this Letter, we propose a method to volumetrically generate relativistically thermal, underdense plasma. Our approach leverages two regimes of magnetically assisted direct laser acceleration (DLA). The energy retained following electron interaction with a short (femtosecond) laser pulse is used to catalyze subsequent heating by a long (picosecond) laser pulse, resulting in a 2D-isotropic momentum spectrum with relativistic average energy over a significant plasma volume. This result is robust to finite laser spot size in the magnetic-field direction, is predicted to occur over a wide range of laser and plasma conditions, and is accessible using current technology. The heating process observed in 2D particle-in-cell (PIC) simulations is consistent with analytic modeling, which predicts that the combined short pulse, long pulse, and applied magnetic field produce multi-MeV plasma that persists for picoseconds following the interaction.

Figures 1(a)–1(c) illustrate the two-stage configuration for generating relativistically thermal plasma. First, a $+x$-propagating, y-polarized relativistic short-pulse laser interacts with electrons in an underdense plasma with an embedded
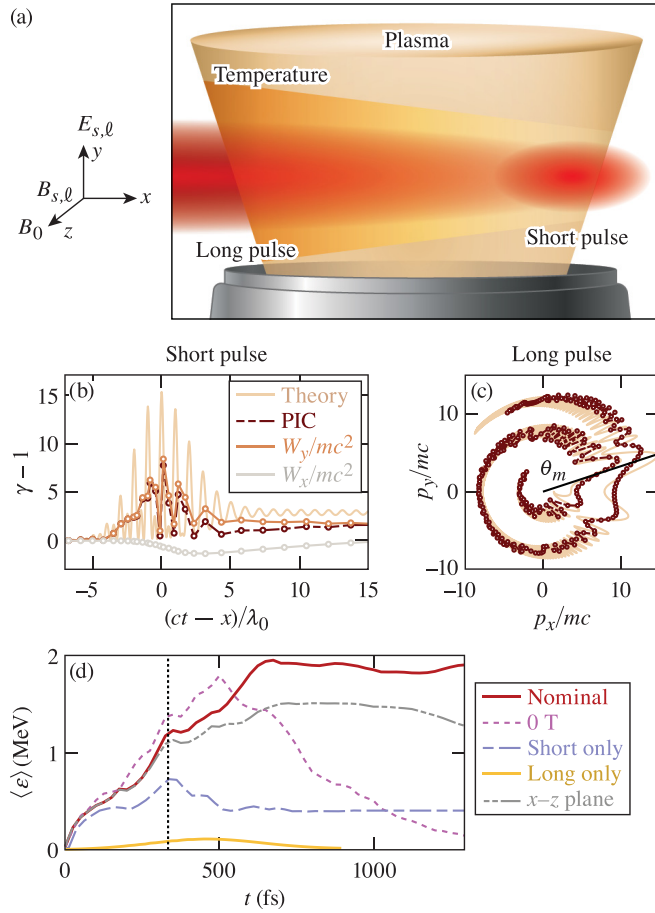
FIG. 1. Generation of relativistic underdense plasma via magnetically assisted direct laser acceleration. (a) Illustration of laser and magnetic-field configuration. [(b), (c)] Example of the energy gain process for a representative electron interacting with (b) the short pulse, and (c) the long pulse. W_y (W_x) is the work done by the transverse (longitudinal) electric field. (d) Average energy of all electrons in $r < 25$ μm. Black dotted line: the time the peak of the short pulse leaves the plasma slab. At the final time shown, the long pulse intensity has dropped to a_ℓ/e at the right edge of the slab. The nominal case corresponds to both laser pulses and $B_{z0} = 500$ T, simulated in the x-y plane.

transverse magnetic field $B_0\hat{\mathbf{z}}$, imparting net energy as electrons slip through the full pulse duration [Fig. 1(b)]. Second, a longer laser pulse with the same propagation and polarization direction interacts with these preheated electrons, delivering half-laser-cycle energy kicks that promote the electron to higher-energy cyclotron orbits [Fig. 1(c)]. The result of these two interactions is a large volume of underdense plasma heated to relativistic energy.

We demonstrate the realization of this hot plasma regime using 2D particle-in-cell simulations. For illustrative purposes, we construct a nominal case using a gas-jet-relevant hydrogen plasma (density $10^{-3}n_c \approx 10^{18}$ cm^{-3}) and weakly focused laser pulses ($f_\# \sim 90$). The short (subscript s) and long (subscript ℓ) laser pulses are weakly to moderately relativistic with a peak normalized electric-field amplitude ($a_0 = |e|E_0/mc\omega_0$, where ω_0 is the laser frequency) of $a_s = 5$ and $a_\ell = 1$. The applied magnetic field is modeled as static and

TABLE I. Nominal 2D simulation parameters. The delay between pulses corresponds to a long-pulse amplitude a_ℓ/e at the peak of the short pulse. Simulations were conducted with high-order cubic B-spline particle shape (which produces robust energy conservation) using the open source particle-in-cell code *EPOCH* [21]. The computational domain was 400 μm$\times$400 μm with open boundary conditions.

Laser parameters	
Laser polarization	y
Propagation direction	$+x$
Wavelength	$\lambda_0 = 1$ μm
Spot size (Gaussian, FWHM in $|E|$)	100 μm
Short pulse	
Duration (Gaussian, FWHM in $|E|$)	$\tau_s = 20$ fs
Peak amplitude	$a_s = 5$
Long pulse	
Duration (Gaussian, FWHM in $|E|$)	$\tau_\ell = 0.8$ ps
Peak amplitude	$a_\ell = 1$
Delay relative to short pulse	$0.6\tau_\ell$
Other parameters	
Applied magnetic field ($\mathbf{B} = B_0\hat{\mathbf{z}}$)	$B_0 = 500$ T
Plasma length	$L = 100$ μm
Electron density	$n_e = 10^{-3}$ n_c
Location of plasma surface	$x = 0$
Time when peak of short pulse is at $x = 0$	$t = 0$
Simulation plane	x–y
Spatial resolution	30 cells/λ_0
Macroparticles per cell, electron/proton	10/5

uniform with $B_0 = 500$ T, conditions which are relevant to laser-driven coil devices [22–25]. Other parameters are given in Table I.

The interaction of the two laser pulses with the target creates multi-MeV average electron energy over a large volume (e.g., $r < w/2 = 25$ μm, where w is the HWHM laser spot size), which persists for picoseconds following the interaction [Fig. 1(d)]. While the plasma can be heated somewhat by the short laser pulse and magnetic field alone, significant relativistic heating requires all three elements of the short laser pulse, long laser pulse, and applied magnetic field [cf., cases in Fig. 1(d)]. The corresponding momentum spectrum is 2D-isotropic [in p_x and p_y, Fig. 2(a)], with a non-Maxwellian, flat energy spectrum [Fig. 2(b)]. Magnetic confinement of hot electrons ensures the density remains close to its starting value ($n_e \approx 0.9 \pm 0.3 \times 10^{-3}n_c$), and suppresses return current. Unlike conventional laser-based heating methods, the flat, relativistic feature ($\gamma \gtrsim 2$) includes more than half of the electron population, i.e., the plasma is relativistically thermal.

These observations are explainable as volumetric heating by magnetically assisted direct laser acceleration in the two distinct regimes covered by the short pulse and the long pulse. While conventional direct laser acceleration in a plane wave (i.e., with $B_0 = 0$) is reversible, the addition of a weak magnetic field transverse to the laser propagation direction slowly rotates the forward electron momentum into transverse momentum and introduces multi-cycle and half-cycle opportunities for irreversible acceleration. During the interaction of an electron with the short pulse, momentum
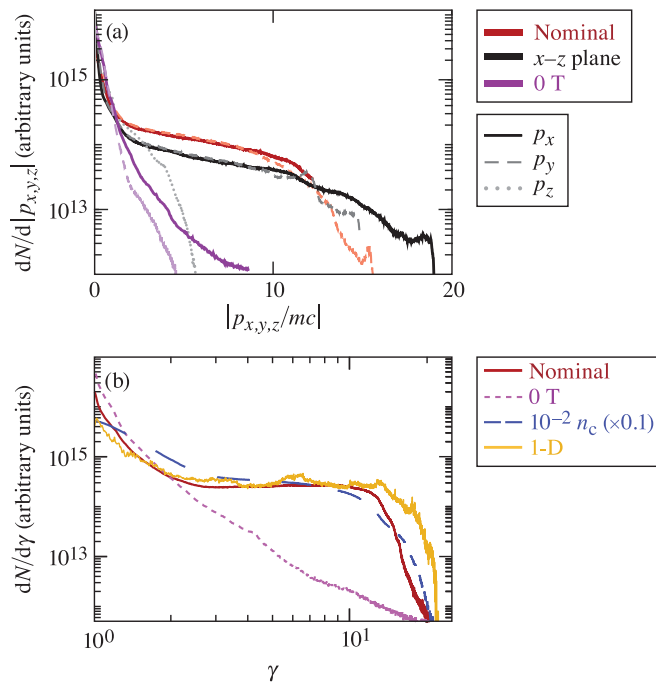
FIG. 2. Characteristic spectra produced by magnetically assisted direct laser acceleration for (a) momentum in each direction and (b) γ. Spectra correspond to $r < 25\,\mu$m and the final time in Fig. 1(d).

rotation by the applied magnetic field changes the dephasing rate $R = \gamma - p_x/mv_\phi$ (where v_ϕ is the phase velocity) over many cycles, allowing the electron to retain energy after the laser has passed [26]. Substantial momentum rotation also occurs during a single half laser cycle when the interaction is sufficiently long [27] and can impart higher net energy than the multi-cycle mechanism. However, entering the necessary regime for half-cycle magnetically assisted DLA by the long pulse requires initial heating, e.g., preheating by the short pulse.

To demonstrate the need for the short pulse to catalyze heating by the long pulse, we write the electron equations of motion (see Supplemental Material [28]) in terms of the evolution of the angle the electron momentum makes with the forward direction, $p_x = |p| \cos\theta$, and the electron energy,

$$\frac{d\gamma}{ds} = \frac{|p_y|}{p_\perp} \frac{\beta \sin\theta}{1 - (\beta/\beta_\phi)\cos\theta} \frac{da}{ds}, \qquad (1)$$

$$\frac{d\theta}{ds} = \frac{|p_y|}{p_\perp} \frac{\frac{\omega_{c0}}{\omega_0} + \frac{1}{\beta}[\cos\theta - \beta/\beta_\phi]\frac{da}{ds}}{\gamma[1 - (\beta/\beta_\phi)\cos\theta]}, \qquad (2)$$

where $s = \omega_0(t - x/v_\phi)$ is the laser phase variable, a is the normalized vector potential, $\omega_{c0} = |e|B_0/m$ is the (nonrelativistic) cyclotron frequency, $p_\perp = \sqrt{p_y^2 + p_{z0}^2}$ (p_z is constant), $\beta_\phi = v_\phi/c$, and $\beta = |p|/\gamma mc$.

Without the applied magnetic field, there is an angle θ_* given by $\cos\theta_* = \beta/\beta_\phi$ which results in $d\theta/ds = 0$ and maximizes the rate of energy gain or loss [Eq. (1)]. The addition of an applied magnetic field modifies the angle for which
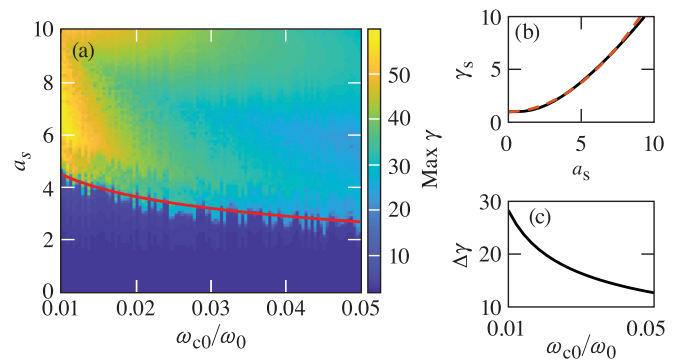

FIG. 3. Threshold for energy gain based on model calculations. (a) Calculated maximum γ with $a_\ell = 1$. Red curve: $\gamma_s = \gamma_0$, where γ_s is the energy retained following interaction with the short pulse, and γ_0 is given by Eq. (4). (b) Black: calculated value of γ_s for the optimum short pulse duration (γ_s is independent of ω_{c0}/ω_0). Red: fit $\gamma_s \approx 1 + 0.11a_s^2$. (c) $\Delta\gamma$ for a single energy kick [Eq. (5)]. In (a), the short-pulse duration was scaled with $(\omega_{c0}/\omega_0)^{-1}$ to maintain the optimal τ_s and the long-pulse duration was scaled with $(\omega_{c0}/\omega_0)^{-3/2}$ to keep τ_ℓ/τ_L constant, where τ_L is the (relativistic) cyclotron period associated with $\Delta\gamma$.

$d\theta/ds = 0$ to [27]

$$\theta \approx \sqrt{2\left(1 - \frac{\beta}{\beta_\phi}\right) + 2\beta\frac{\omega_{c0}}{a_\ell\omega_0}} = \sqrt{\theta_*^2 + \theta_m^2}, \qquad (3)$$

in the small angle limit, with $da/ds \sim a_\ell$ and $\theta_m \equiv \sqrt{2\beta\omega_{c0}/a_\ell\omega_0}$. When $\theta_m \gtrsim \theta_*$, Eqs. (1) and (2) predict half-cycle acceleration with the constant angle θ_m, in good agreement with both observed electron trajectories and those calculated from the solution to the electron equations of motion in the vacuum plane wave limit [Fig. 1(c)].

However, $\theta_m \gtrsim \theta_*$ requires electrons be heated prior to the interaction. The initial γ_0 needed to catalyze half-cycle acceleration is approximately

$$\gamma_0 \gtrsim f\sqrt{\frac{a_\ell}{2}\frac{\omega_0}{\omega_{c0}}}, \qquad (4)$$

where f is given by $f = \exp(-2a_\ell f)$, and accounts for acceleration near $\theta = 0$ (see Supplemental Material [28]). For $a_\ell = 1$, $\gamma_0 \gtrsim 0.3\sqrt{\omega_0/\omega_{c0}}$.

In the two-laser configuration, preheating is provided by the short pulse through many-cycle magnetically assisted DLA [26] [illustrated for a single electron in Fig. 1(b)]. Equation 4 introduces a threshold in the short pulse intensity needed to catalyze heating by the long pulse, which is illustrated in the vacuum plane wave limit (scanning over the initial laser phase) in Figs. 3(a) and 3(b). The a_s used in simulations is significantly above this threshold, which makes the heating process robust to wakefield formation. The predominant effect of wakefield formation is to reduce the energy retained by electrons following interaction with the short pulse, via the detrimental effect of the decelerating plasma electric field on direct laser acceleration [difference between W_y and the theoretical value in Fig. 1(b)]. Overall, the longitudinal electric field makes no net contribution to the

energy for the majority of electrons during acceleration by either the short or long pulses.

The maximum half-cycle energy kick the long pulse can provide is [27]

$$\Delta\gamma \sim 2^{3/2}\, a_\ell^{3/2} \sqrt{\frac{\omega_0}{\omega_{c0}}}, \qquad (5)$$

obtained by integrating Eq. (1) over half a laser cycle in the small angle limit with $\theta \approx \theta_m$, $\beta \approx 1$, and $p_{z0} = 0$ [Fig. 3(c)]. The energy imparted by the accelerating halfcycle is at least partly retained during subsequent laser cycles [the rate of energy transfer in Eq. (1) decreases with increasing θ]. Cyclotron rotation eventually returns the electron to favorable conditions for energy exchange where it can get another large kick from the laser, either promoting the electron to a yet-higher energy orbit [as can be seen in Fig. 1(c)] or resulting in energy loss. Although electrons typically undergo more than one half-cycle energy kick in the nominal simulation, the cutoff energy (where $dN/d\gamma$ drops rapidly) remains comparable to $\Delta\gamma$ [Fig. 2(b)].

While 2D simulation demonstrates the feasibility of producing multi-MeV relativistically thermal plasma under experimentally relevant conditions, the parameters chosen for these simulations (to maintain tolerable computational cost) produce sub-optimal plasma heating. One-dimensional simulation yields a nearly identical hot-electron spectrum as the 2D case [$\gamma \gtrsim 2$ in Fig. 2(b); i.e., the heating mechanism is fundamentally 1D-like] but overpredicts the average electron energy by $\sim 2\times$, due to lower return current in the 1D case (in 2D, return current electrons primarily originate at radii outside the central spot). Nevertheless, 1D simulations indicate that even hotter plasma can be generated by increasing the plasma size and long-pulse duration, and that heating can be facilitated by weaker applied magnetic fields.

First, increasing the plasma size increases the average electron energy by reducing electron interaction with the plasma-vacuum boundary. The plasma length in 2D simulations $L = 100\ \mu m$ is comparable to the Larmor radius of hot electrons $\rho_L \sim c\Delta\gamma/\omega_{c0}$, allowing a significant portion of electrons to encounter the decelerating sheath electric field during their acceleration, which is detrimental to the half-cycle energy gain process. Increasing the plasma size results in saturation of the average electron energy at a few times the Larmor radius [Fig. 4(a)].

Second, increasing the pulse duration increases the number of half-cycle energy kicks electrons receive, which increases the cutoff energy of the flat spectral feature. The long-pulse duration used in 2D simulations is comparable to the cyclotron period of hot electrons ($\tau_\ell \sim \tau_L$, where $\tau_L \approx 2\pi \rho_L/c$), allowing most electrons to receive one or two significant energy kicks. As the pulse duration is increased, additional kicks are allowed, increasing both the cutoff and the average electron energy [Fig. 4(b)].

Lastly, relativistically thermal plasma can still be produced at lower, pulsed-power-relevant [29–34] magnetic field strength. Simulations conducted with a 200-T magnetic field and scaled pulse durations ($\omega_{c0}\tau_s$ and τ_ℓ/τ_L kept constant) exhibit similar saturation behavior with increasing L [Fig. 4(a)] and similar scaling with pulse duration in the saturated regime
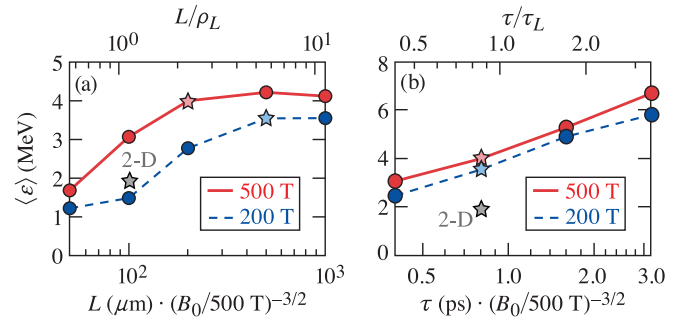

FIG. 4. Strategies for improving average electron energy in 1D PIC simulations. (a) Scan over plasma size near $L/\rho_L \sim 1$ with fixed duration. (b) Scan over long-pulse duration near $\tau_\ell/\tau_L \sim 1$ with fixed plasma size. ρ_L and τ_L are the Larmor radius and cyclotron period associated with $\Delta\gamma$. The starred points are shared between (a) and (b). The peak of the short pulse is kept coincident with a_ℓ/e on the rising edge of the long pulse. $\tau_s = 50$ fs for the 200-T cases.

[Fig. 4(b)] as the 500-T case. In agreement with Eq. (5), the magnetically assisted DLA spectral feature extends to higher energy in the 200-T case. However, the average electron energy is somewhat lower due to fewer electrons meeting the preacceleration requirement for the same a_s, as a result of higher γ_0 and stronger wakefield generation (due to longer pulse duration and elimination of the weak $\sim 10\%$ wake damping from the small Larmor radius in the 500 T case.)

The two-pulse magnetically assisted DLA process is robust to additional experimental considerations, including increasing the plasma density by an order of magnitude [2D $10^{-2}\ n_c$ case in Fig. 2(b)], decreasing the laser spot size by a factor of two, and finite spot size in the magnetic field (z) direction. 2D simulation in the x-z plane (which introduces electron motion along magnetic field lines) features the same acceleration process as the nominal case and also produces a 2D-isotropic momentum spectrum [Fig. 2(a)], albeit with somewhat reduced average energy [e.g., Fig. 1(d)]. The finite spot size in the magnetic-field direction additionally sets a picosecond time scale for dissipation of the hot plasma (based on 100-μm-scale spot size and the observed $\langle p_z \rangle / \langle \gamma \rangle mc \approx 0.16$).

Both stages of magnetically assisted direct laser acceleration are also robust to departure from the idealized initial conditions of zero initial electron temperature and plasma and magnetic field uniformity. In simulations replicating the 1D, 500 T starred configuration in Fig. (4), the final electron spectrum and average energy remained unchanged with nonrelativistic initial electron temperature, even beyond what might realistically be expected (e.g., 10 keV). Adding a 50 μm linear density ramp to either side of the plasma slab also had negligible effect. Spatial variation in the magnetic field changes the optimum conditions for acceleration, but significant variation within the slab is required to substantially change the plasma heating (the average electron energy remains within 15% of the uniform case when the field is varied by $\sim 25\%$, using a frozen in $\sin^2$ magnetic field profile).

As a final note, the two-pulse scheme is advantageous relative to plasma heating by the short pulse alone. $\Delta\gamma$ is

higher than the energy retained following interaction with the short pulse (γ_s), even if the combined pulse energy is given entirely to the short pulse [i.e., $a_s = 8$, compare Figs. 3(b) and 3(c)]. In both 1D and 2D simulations, both the cutoff and average electron energy are substantially higher with the two-pulse scheme (cf., average energy of 1.9 MeV versus 1.1 MeV for the nominal 2D case), and the characteristic flat energy feature [shown in Fig. 2(b)] is only observed when both pulses are present. In addition, the two-stage process and the relativistically thermal plasma it produces is ideal to investigate astrophysical processes such as maser radiation [11] and the cosmic ray injection problem [35].

Our 1D and 2D simulations demonstrate that generation of underdense, relativisitically thermal plasma can be realized with state-of-the-art or near-term laser [36–39] and magnetic-field-generation capabilities [25,31]. Magnetic fields from 200 T to 500 T enable multi-MeV average electron energy under gas-jet relevant conditions, using kilojoule-class multipicosecond pulses and 10 Joule to kilojoule-class femtosecond pulses, with an acceleration process that reproduces important features of cosmic ray acceleration. Plasma heating by magnetically assisted direct laser acceleration is thereby anticipated to offer the first practical access to the relativistically thermal plasma regime, introduce a new laboratory analog for studying astrophysical particle acceleration, and enable experimental verification of longstanding, foundational predictions in basic plasma physics, laser-plasma physics, and laboratory astrophysics.

[1] J. Bergman and B. Eliasson, Linear wave dispersion laws in unmagnetized relativistic plasma: Analytical and numerical results, Phys. Plasmas **8**, 1482 (2001).

[2] M. Lontano, S. Bulanov, and J. Koga, One-dimensional electromagnetic solitons in a hot electron-positron plasma, Phys. Plasmas **8**, 5113 (2001).

[3] T. B. Yang, J. Arons, and A. B. Langdon, Evolution of the weibel instability in relativistically hot electron-positron plasmas, Phys. Plasmas **1**, 3059 (1994).

[4] D. J. Stark *et al.*, Relativistic Plasma Polarizer: Impact of Temperature Anisotropy on Relativistic Transparency, Phys. Rev. Lett. **115**, 025002 (2015).

[5] G. Li, W. B. Mori, and C. Ren, Laser Hosing in Relativistically Hot Plasmas, Phys. Rev. Lett. **110**, 155002 (2013).

[6] Y. Zhao *et al.*, Effects of relativistic electron temperature on parametric instabilities for intense laser propagation in underdense plasma, Phys. Plasmas **21**, 112114 (2014).

[7] J. S. Ross *et al.*, Observation of Relativistic Effects in Collective Thomson Scattering, Phys. Rev. Lett. **104**, 105001 (2010).

[8] T. Katsouleas and J. M. Dawson, Unlimited Electron Acceleration in Laser-Driven Plasma Waves, Phys. Rev. Lett. **51**, 392 (1983).

[9] G. N. Kichigin, The surfatron acceleration of cosmic rays in the galactic plasma, J. Exp. Theor. Phys. **92**, 895 (2001).

[10] L. Gargaté, R. A. Fonseca, L. O. Silva, R. A. Bamford and R. Bingham, SEP acceleration in CME driven shocks using a hybrid code, Astrophys. J. **792**, 9 (2014).

[11] R. Bingham, B. J. Kellett, R. A. Cairns, J. Tonge, and J. T. Mendonca, Cyclotron maser radiation from astrophysical shocks, Astrophys. J. **595**, 279 (2003).

[12] B. D. Metzger, B. Margalit, and L. Sironi, Fast radio bursts as synchrotron maser emission from decelerating relativistic blast waves, Mon. Not. R. Astron. Soc. **485**, 4091 (2019).

[13] M. A. Purvis *et al.*, Relativistic plasma nanophotonics for ultrahigh energy density physics, Nat. Photon. **7**, 796 (2013).

[14] S. M. Weng *et al.*, Dense blocks of energetic ions driven by multi-petawatt lasers, Sci. Rep. **6**, 22150 (2016).

[15] L. Fedeli, A. Formenti, L. Cialfi, A. Pazzaglia, and M. Passoni, Ultra-intense laser interaction with nanostructured near-critical plasmas, Sci. Rep. **8**, 3834 (2018).

[16] G. Li *et al.*, Laser Channeling in Millimeter-Scale Underdense Plasmas of Fast-Ignition Targets, Phys. Rev. Lett. **100**, 125002 (2008).

[17] T. Tajima and J. M. Dawson, Laser Electron Accelerator, Phys. Rev. Lett. **43**, 267 (1979).

[18] E. Esarey, C. B. Schroeder, and W. P. Leemans, Physics of laser-driven plasma-based electron accelerators, Rev. Mod. Phys. **81**, 1229 (2009).

[19] J. Kruger and M. Bovyn, Relativistic motion of a charged particle in a plane electromagnetic wave with arbitrary amplitude, J. Phys. A: Math. Gen. **9**, 1841 (1976).

[20] F. V. Hartemann *et al.*, Nonlinear ponderomotive scattering of relativistic electrons by an intense laser field at focus, Phys. Rev. E **51**, 4833 (1995).

[21] T. D. Arber *et al.*, Contemporary particle-in-cell approach to laser-plasma modelling, Plasma Phys. Controlled Fusion **57**, 113001 (2015).

[22] L. Gao *et al.*, Ultrafast proton radiography of the magnetic fields generated by a laser-driven coil current, Phys. Plasmas **23**, 043106 (2016).

[23] C. Goyon *et al.*, Ultrafast probing of magnetic field growth inside a laser-driven solenoid, Phys. Rev. E **95**, 033208 (2017).

[24] S. Fujioka *et al.*, Kilotesla magnetic field due to a capacitor-coil target driven by high power laser, Sci. Rep. **3**, 1170 (2013).

[25] J. J. Santos *et al.*, Laser-driven strong magnetostatic fields with applications to charged beam transport and magnetized high energy-density physics, Phys. Plasmas **25**, 056705 (2018).

[26] A. P. L. Robinson and A. V. Arefiev, Net energy gain in direct laser acceleration due to enhanced dephasing induced by an applied magnetic field, Phys. Plasmas **27**, 023110 (2020).

[27] A. Arefiev, Z. Gong, and A. P. L. Robinson, Energy gain by laser-accelerated electrons in a strong magnetic field, Phys. Rev. E **101**, 043201 (2020).

[28] See Supplemental Material at http://link.aps.org/supplemental/10.1103/PhysRevResearch.4.L042017 for the derivation of Eqs. (1) and (2), and the factor f in Eq. (4).

[29] O. Portugall *et al.*, Megagauss magnetic field generation in single-turn coils: new frontiers for scientific experiments, J. Phys. D **32**, 2354 (1999).

[30] V. V. Ivanov *et al.*, Experimental platform for investigations of high-intensity laser plasma interactions in the magnetic field of a pulsed power generator, Rev. Sci. Instrum. **89**, 033504 (2018).

[31] V. V. Ivanov *et al.*, Generation of strong magnetic fields for magnetized plasma experiments at the 1-ma pulsed power machine, Matter Radiat. Extremes **6**, 046901 (2021).

[32] G. Fiksel *et al.*, Note: Experimental platform for magnetized high-energy-density plasma studies at the omega laser facility, Rev. Sci. Instrum. **86**, 016105 (2015).

[33] G. Fiksel *et al.*, Inductively coupled 30 t magnetic field platform for magnetized high-energy-density plasma studies, Rev. Sci. Instrum. **89**, 084703 (2018).

[34] J. Peebles and D. Mastrosimone, Performing omega experiments with non-standard targets, Presented at: OMEGA Users Group Meeting (2019).

[35] K. G. McClements, M. E. Dieckmann, A. Ynnerman, S. C. Chapman, and R. O. Dendy, Surfatron and Stochastic Acceleration of Electrons at Supernova Remnant Shocks, Phys. Rev. Lett. **87**, 255002 (2001).

[36] D. N. Maywar *et al.*, OMEGA EP high-energy petawatt laser: progress and prospects, J. Phys.: Conf. Ser. **112**, 032007 (2008).

[37] I. A. Begishev *et al.*, Advanced laser development and plasma-physics studies on the multiterawatt laser, Appl. Opt. **60**, 11104 (2021).

[38] S. Borneis *et al.*, Design, installation and commissioning of the eli-beamlines high-power, high-repetition rate hapls laser beam transport system to P3, High Power Laser Sci. Eng. **9**, e30 (2021).

[39] N. Jourdain *et al.*, The l4n laser beamline of the p3-installation: Towards high-repetition rate high-energy density physics at eli-beamlines, Matter Radiat. Extremes **6**, 015401 (2021).

[40] J. Towns *et al.*, XSEDE: Accelerating scientific discovery, Comput. Sci. Eng. **16**, 62 (2014).